Research Article Vol. 37, No. 2 / February 2020 / Journal of the Optical Society of America B 433

Journal of the Optical Society of America B

OPTICAL PHYSICS

Transient grating measurements at ultralow probe power

Baozhu Lu,[1,2] Mykola Abramchuk,[3] Fazel Tafti,[3] and Darius H. Torchinsky[1,2,*]

[1]Department of Physics, Temple University, Philadelphia, Pennsylvania 19122, USA
[2]Temple Materials Institute, Temple University, Philadelphia, Pennsylvania 19122, USA
[3]Department of Physics, Boston College, Chestnut Hill, Massachusetts 02467, USA
*Corresponding author: dtorchin@temple.edu

Received 11 September 2019; revised 12 December 2019; accepted 20 December 2019; posted 23 December 2019 (Doc. ID 377545); published 28 January 2020

We report on an ultralow probe-power transient grating apparatus with probing based on a laser diode pulser, a digital delay generator, and a data acquisition card. The electronic triggering of the diode pulser permits stroboscopic measurement of arbitrarily slow laser-induced dynamics using pulses of probe light with average power ∼5 nW, significantly lower than what is currently used by continuous wave measurement. The proposed method also allows for flexibility in selection of the probe wavelength limited only by availability of low threshold current laser diodes. Examples of impulsive stimulated thermal scattering measurements are presented on liquid isopropanol, single crystal solid $CrCl_3$, and a thin film of Cu vapor deposited on a Si substrate, demonstrating the flexibility of the technique. © 2020 Optical Society of America

https://doi.org/10.1364/JOSAB.377545

1. INTRODUCTION

The transient grating (TG) technique has been established as a mainstay spectroscopic tool owing to its applicability to a broad array of phenomena [1]. On short time scales (10 fs–1 ns), TG measurements permit the study of, e.g., electronic excited state lifetimes [2,3], diffusion of electronic quasiparticles [4,5], and propagating excitations such as optical phonon and polariton modes [6,7]. Application to longer time scale (1 ns–1 ms) processes is no less diverse, with TG experiments revealing various relaxation dynamics of viscoelastic media [8–12], the mechanical properties of thin films [13,14] and single crystals [15,16], as well as the interplay between magnetism and elasticity [17–19]. Studies have also revealed the longitudinal viscosity of nanofluids [20] and the evolution of the mechanical moduli of materials under the conditions of static high pressure [21,22] and shock loading [23]. TG has even been used to observe ballistic thermal transport in silicon [24], record phonon mean free paths [25], measure second sound propagation in graphite [26], and determine the thermal diffusivity of thin films [27]. Through-plane thermal diffusion can also be observed [28].

Although the TG excitation process can be easily performed using a variety of sources including, e.g., Ti:sapphire, Nd:YAG, and passively Q-switched diode lasers [29], the probing process presents multiple challenges that serve as significant limitations of the technique. Excitations on the $\lesssim 1$ ns time scale must be measured using a "pulsed probe" configuration, where the probe laser comprises a low-power, mechanically delayed portion of the original driving laser. A benefit of this approach is that the use of a 100 fs time scale probe allows for a high peak intensity that can be used to detect weak signals at only moderate average power, limiting sample heating while simultaneously providing a high density of photons per unit time interval of signal. However, pulsed probing is only of limited utility for slow dynamics, as temporal windows $\gtrsim 30$ ns require prohibitively long optical delay lines.

In principle, the issue of a limited temporal window may be addressed by the use of high bandwidth electronic detectors and continuous wave (CW) laser-based probing. A strength of this method is that the entire data trace may be acquired at one time as opposed to point by point as in pulsed probing. Nevertheless, the peak photon yield of CW probing is often much weaker than that of pulsed probing. With fewer photons per unit time interval of signal, this scheme typically requires high-gain detection electronics and the use of optical heterodyning techniques to measure the photoinduced dynamics [30]. Thus, CW probing may also necessitate ∼100 mW average laser power in the probe beam alone, presenting a significant heat load to nontransparent media. The need for such high average power restricts the selection of usable probe wavelengths to those for which strong, single transverse optical mode diode lasers are available. Gating the probe beam through an electro-optic modulator can reduce this heat load significantly for short-lived excitations by limiting its relative duty cycle to the time window of the relatively short acoustic signal being measured, producing thermal loads as low as ∼100 μW, but is not feasible for long-lived responses.

Another challenge to CW detection is the proper selection of the detector and associated electronics. The measurement of phenomena that span the 1 ns–1 ms time scales requires high bandwidth, and thus noisier, AC-coupled detectors connected to high bandwidth oscilloscopes in parallel with bandwidth-limited DC-coupled devices to observe the slower dynamics. The data must then be matched in software to reconstruct the full time-domain response. Furthermore, the use of DC-coupled detectors is complicated by an unstable baseline signal level driven by thermal drift and laser pointing fluctuations deriving from air currents. This optical instability makes data acquisition difficult, especially for very slow processes or weak signals.

Here, we describe the design and construction of a novel TG device that effectively surmounts the issues of thermal loading by the probe beam, challenging accessibility to expensive, high-power laser diodes at different wavelengths, and the need to use two different types of detectors to access the different time scale responses. Our design hinges on using an electronically triggered diode laser pulser capable of generating tunable pulse width laser pulses as short as 100 ps in duration or as long as 2 ns. As the delay between the pump and probe pulses is electronic instead of mechanical, our device does not suffer from the limitations set by delay stage length. From the specified jitter of 12 ps, the apparatus potentially allows detection of acoustic waves up to ∼5 GHz in frequency. Due to the ultralow duty cycle of the diode pulser, the average power incident upon the sample is limited to the nW regime, significantly mitigating probe-laser-based heating. The pulser also allows for use of affordable arbitrary wavelength laser diodes, permitting use in spectroscopic applications, and allows for the use of low-noise, narrow-bandwidth detectors. Below, we demonstrate our technique by measuring the mechanical and thermal properties of a liquid, the longitudinal modulus of a transparent single crystal, and the thickness of a vapor-deposited thin film for temporal windows limited in duration only by the pulse to pulse time interval of the laser, with measured acoustic frequencies in the range of ∼50−900 MHz.

2. EXPERIMENTAL DESIGN AND CONSIDERATIONS

In a typical TG measurement, depicted schematically in Fig. 1, a pulse from a pump laser of wavelength λ_e is split into two equal portions that are crossed at an angle θ relative to one another in the sample, forming an interference pattern, or "grating," of wavelength $\Lambda = \lambda_e/(2\sin(\theta/2))$ that in turn creates a spatially periodic, transient change in the index of refraction. This excitation is measured by recording the time-dependent intensity of a second laser diffracted at Bragg angle from this TG, as shown in Fig. 1(b).

Figure 2 shows a top-down experimental layout of the device with a side-on portion in the inset. A beam from a 5 kHz regeneratively amplified Ti:sapphire laser was used to pump an optical parametric amplifier (Light Conversion, TOPAS Twins) to produce an excitation beam of wavelength $\lambda_e = 480$ nm − 2.6 μm, where λ_e was chosen to be absorbed by the medium under study. The pump and probe beams were then focused by a 20 cm cylindrical lens (Thorlabs, LJ1653L1-B) onto a diffractive optic comprising several different binary phase mask patterns of wavelength Λ ranging from 1 μm to 200 μm (Tessera, Custom) to provide the ±1 orders of diffraction of both beams that were recombined onto the sample, allowing heterodyne detection with the probe [31]. After the phase mask, the beams were recollimated by a reflective spherical optic, and then focused by a second spherical reflector (Thorlabs, CM508-200-P01 and CM508-150-P01, consecutively) with a 4:3 imaging ratio onto the sample. Since the laser beams form a line-shaped focus on the phase mask from the cylindrical lens, the two-lens telescope formed by the spherical reflectors creates an interference pattern that incorporates several fringes, resulting in long-lived acoustic responses. After interacting with the sample, the pump beam was blocked by a piece of black paper. Any remaining residual pump scatter was removed using long- or short-pass filters that transmitted the probe wavelength only (Thorlabs, various FESH and FELH series filters).

Two different chopping schemes were used to modulate the pump beam. In the first, we chopped the pump amplitude at half the laser repetition rate using a chopper wheel. In the second approach, we modulated the pump beam by phase rather than by amplitude. This was accomplished by placing a ∼125 μm thick fused silica coverslip (Valley Design, FS-226) manually cut with a diamond scribe to a size such that it intersected only one arm of the pump beam at a 45° angle as depicted in the Fig. 2 inset. The cut coverslip was attached to a galvanometer (Pangolin Laser Systems, Saturn 1B) by Pangolin Laser Systems. This galvanometer oscillated the coverslip at half the laser frequency such that it introduced a π phase delay in one pump arm relative to the other on every other pulse, effectively reversing the sign of the impulsive stimulated thermal scattering (ISTS) signal. We also took care to place the same thickness of glass into the second pump arm so that both pump pulses would arrive at the sample simultaneously. We observed that this produced unstable signals for excitation wavelengths $\lambda_e < 1.2$ μm, which

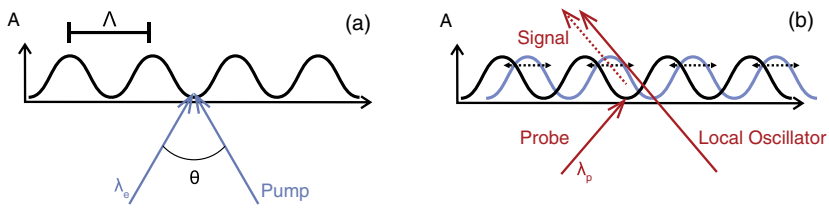

Fig. 1. Representation of the TG process. (a) Pump beams of wavelength λ_e crossed at an angle θ produce a grating of wavelength $\Lambda = \lambda_e/(2\sin(\theta/2))$. (b) The probe beam diffracts off of propagating excitations and the slowly decaying grating with the signal amplified by a local oscillator field in the heterodyne configuration.

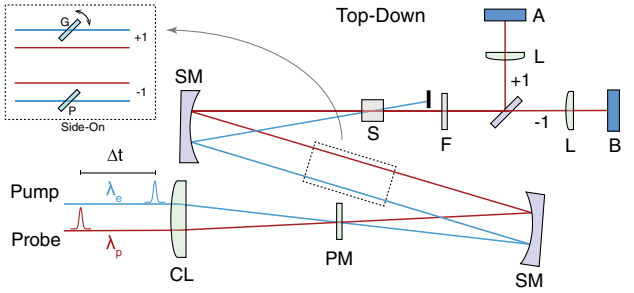

Fig. 2. Top-down diagram of ISTS setup with side-on inset. CL, cylindrical lens; PM, phase mask; SM, spherical mirror; S, sample; F, filter; L, lens; A and B, photodiode detectors; G, galvanometer mounted coverslip; P, phase and delay compensating coverslip.

we posit is due to the impact on the optical phase from the mechanical instability produced by oscillating a very thin piece of glass at extremely high frequencies. However, this method provided a better signal-to-noise ratio (SNR) than amplitude chopping for $\lambda_e > 1.2$ μm, for which the optical wavelength was long enough such that the optical phase was not impacted by this instability.

The probe laser consisted of a laser diode pulser (Highland Technology, T165-2) specified to deliver 700 mA current transients into a laser diode over a tunable 100 ps to 2 ns time span as triggered by an external digital delay generator (Highland Technology, T560). The bias and current settings of the T165-2 were chosen for maximum output through electronic control by a data-acquisition card-based (DAC) control board (MCCDAQ, USB-3101). The timing window, which set the optical width of the pulse, was picked to generate the shortest possible pulse that was still detectable, corresponding to roughly above the lasing threshold for all wavelengths used. We did not have access to adequate high bandwidth electronics to measure this pulse duration.

In performing this study, we tested several laser diodes at the following probe wavelengths λ_p (all part numbers in parentheses from Thorlabs): 405 nm (L405P20 and DL5146-101S), 520 nm (L520P50), 635 nm (L635P5), 650 nm (L650P007), 785 nm (L785P050), 808 nm (L808P101 and L808P200), 833 nm (HL8338MG), 904 nm (L904P010), and 980 nm (L980P010). The only laser diode that did not work in our apparatus was a diode-pumped solid-state laser (Thorlabs, DJ532-10), which we posit is because there was insufficient photon yield to produce a population inversion in the $Nd:YVO_4$ lasing medium. Eventually, we settled for probe wavelengths $\lambda_p = 405$, 635, and 808 nm as these were minimally absorbed by the materials we investigated. The visible wavelengths were easy to work with since their reflections from a business card were clearly visible to the naked eye when the diode pulser was run with maximum pulse width. In contrast, the infrared (IR) laser diodes were difficult to use since the output power was so low as to be dim even when viewed by a sensitive IR viewer (FJW, FIND-R-SCOPE 89400).

The 635 nm laser diode (Thorlabs, L635P5) and the 808 nm laser diode (Thorlabs, L808P101) were each separately placed into collimation packages (Thorlabs, LT230P-B) that were modified so that the end of the diode could be placed flush with the driver board. The laser diodes were thus directly plugged into the board to reduce circuit inductance and capacitance and eliminate oscillations in the output amplitude. For small diode packages, we found it sufficient to splay the diode leads wide enough to fit into a photodiode socket (Thorlabs, S8060) before attaching to the pulser, while 9 mm laser diodes could be plugged into the device directly. The 405 nm laser diode (Thorlabs, L405P20) was integrated into a fiber-coupled pigtailed diode package (Oz Optics, LDPC-02-405-3/125-S-40-3A-1-1-30-CSP:L405P20) by Oz Optics that was then directly plugged into the pulser board. This diode was collimated by a screw-on optic (Thorlabs, F671APC-405), providing a narrow, low-divergence Gaussian output.

Although the T165-2 specifies that it provides 700 mA over the duration of the laser pulse, we found that laser diodes with low maximum operating current (∼30 mA) could be run at the full 700 mA with the longest available pulse width. This allowed us to purchase affordable laser diodes with low threshold current, which we noticed produced cleaner signals than high threshold current diodes. We attribute the robustness of the laser diodes to the fact that their primary failure mode is heating, which results in catastrophic optical damage (COD) [32–34]. At the 5 kHz repetition frequency used here, the duty cycle of the laser diode is approximately 5×10^{-6}, which is sufficiently low to avoid heating-induced COD for most laser diodes. When the duty cycle was increased to $\sim 1 \times 10^{-4}$, some of the laser diodes failed irretrievably, further suggesting low duty cycle as important to proper diode function. However, even at the lowest duty cycles used, we noticed that a handful of the 635 nm laser diodes we tested could only generate TEM_{01} output after a long period of use. We observed that each of the two output antinodes appeared to contribute ISTS signal of opposite optical phase that nearly canceled to zero, which we addressed by spatially filtering out one of the antinodes through a pinhole aperture.

After interacting with the sample, both probe fields were focused onto photodiodes (Hamamatsu S5973-02) that were connected to charge-sensitive preamplifiers (Cremat, CR-Z-110) with a specified gain of 1.4 V/pC. The outputs of the two preamplifiers were input into a shaping instrument (Cremat, CR-S-8us) to convert the charge-integrated signal into a Gaussian voltage pulse. Data were acquired using a DAC balanced detection scheme [35] that we found to be better suited to this measurement—and faster—than lock-in detection. This required that the output of the shaper be connected to the inputs of a DAC (National Instruments, NI PCI-6143) via by a shielded cable (National Instruments, SHC68-68-EPM) to its breakout box (National Instruments, BNC-2110).

3. RESULTS AND DISCUSSION

The TG response we focused on here is ISTS, which probes the $\sim 1 - 100$ μm length scale thermal and mechanical properties of liquid and solid materials through the heat-driven generation of acoustic waves. In the ISTS process, the absorbed light is transferred into heat in the sample on the 1–10 ps time scale, raising the local temperature and resulting in an immediate thermal expansion profile matching the sinusoidal excitation pattern. This thermal expansion generates a modulated strain profile that launches counterpropagating

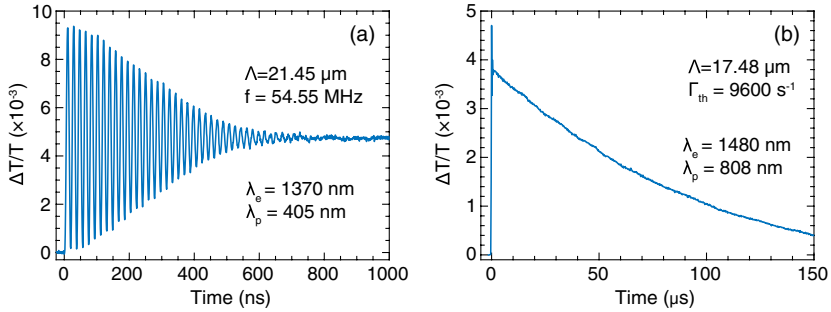

Fig. 3. ISTS data in isopropanol. (a) Acoustic data comprising 1020 data points taken with a 1 ns time step. The decay of the acoustic oscillations is governed by acoustic wave propagation away from the probed area as opposed to intrinsic damping. (b) Thermal data comprise 170 data points taken with a 5 ns time step. In both cases, data acquisition lasted ∼2 min.

acoustic waves of wavelength Λ or, equivalently, wave vector $q = 2\pi/\Lambda$. Longitudinal acoustic waves are generated in the bulk of the material in the case of weakly absorbing media, while for strongly absorbing samples with short optical penetration depths, the excitation comprises a surface acoustic wave whose strain profile penetrates on order $\sim q^{-1}$ into the sample. Simultaneous to these acoustic responses, the thermal excitation grating diffuses from the interference pattern peaks to nulls exponentially at a rate $\Gamma_{\text{th}} = Dq^2$, where D is the thermal diffusivity.

We tested our TG apparatus by performing ISTS measurements on three representative material systems: a transparent liquid sample of isopropanol, a transparent, magenta single crystalline sample of $CrCl_3$, and a copper thin-film vapor deposited onto a silicon substrate. Raw data traces from these various materials are shown in Figs. 3–5 and were numerically Fourier transformed in order to determine the acoustic frequency. In the case of the thin film, up to three acoustic frequencies were simultaneously observed deriving from the simultaneous excitation of multiple pseudo-Rayleigh modes, permitting an analysis to determine the thickness of the film, as described below.

Although a significantly better SNR may be obtained with an attenuated heterodyne, in which the local oscillator field is reduced by several orders of magnitude to suppress the background component and its associated noise, we used an unattenuated heterodyne to allow for maximum detection bandwidth. In doing so, we often used the laser diodes at the limit of detectable output to minimize the probe pulse duration, resulting in light pulses that were too weak to be attenuated by a ND2 or ND3 filter as required for attenuated heterodyne. Using the specified parameters of the detection electronics described above, we estimate that there were roughly 10^6 photons/pulse in this configuration. We remark that if we had used photomultiplier tubes instead of photodiodes for detection, the photon flux could have been further reduced to allow for either measurement of faster dynamics with shorter pulses or attenuated heterodyne detection to improve the SNR.

A. Liquid Measurements

Isopropanol was obtained from Sigma Aldrich and used without further purification. The liquid was poured into a UV fused

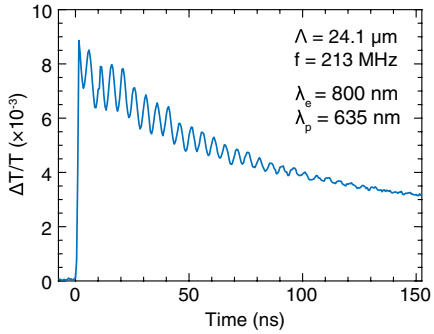

Fig. 4. ISTS data on $CrCl_3$. The data comprise 321 data points taken with a 500 ps time step and required 5 min of averaging. The acoustic amplitude is considerably smaller relative to a large, slowly decaying background.

quartz cuvette (Thorlabs, CV10Q3500F-E) with 10 mm transmitted path length. Two different experimental configurations were used. In the first, the excitation wavelength was chosen at $\lambda_e = 1370$ nm to correspond to weak absorption into the first overtone of the O–H stretching mode at 3650 cm^{-1}, which allowed the use of only 2.8 mW of power at the sample, corresponding to 560 nJ/pulse. The 405 nm, fiber-coupled laser diode described above was used as the probe beam in the unattenuated heterodyne configuration. In the second, we acquired data using $\lambda_e = 1480$ nm excitation and the $\lambda_p = 808$ nm probe laser with similar pulse energies. In order to prevent blooming of the liquid as well as white light continuum generation and self-focusing of the beam, the pump pulse was temporally dispersed by transmission through a ∼15 cm thick piece of glass (Newlight Photonics, SF11L1150), which suppressed nonlinear interaction of the laser with the liquid but still allowed the excitation beam to be impulsive relative to the acoustic period. All data on the liquid were taken using the galvanometer as a modulator in the pump arm to "chop" the pump beam at 2.5 kHz while the 5 kHz repetition rate probe beam recorded data with synchronous delay time scanning.

The raw acoustic data are plotted in Fig. 3(a) for a grating period of 21.45 μm using pump excitation wavelength $\lambda_e = 1370$ nm and probe wavelength $\lambda_p = 405$ nm. The data show a time-domain trace of an oscillating signal at 54.55 MHz where the disappearance of the signal is primarily governed by

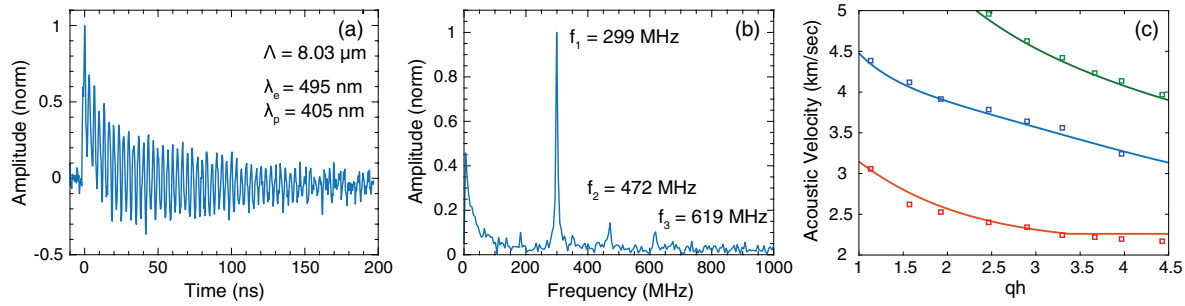

Fig. 5. ISTS data for a 3.2 μm film of Cu evaporatively coated on Si comprising 538 data points taken with a 400 ps time step, necessitating ∼7 min of data acquisition. (a) Time-domain signal for acoustic wavelength $\Lambda = 8.03$ μm. (b) Fourier transform of the time-domain signal in panel (a) showing three acoustic modes at the labeled frequencies. (c) Fits to the measured acoustic dispersion curves for the three observed acoustic branches.

acoustic wave walk-off rather than by damping, as apparent from the Gaussian shape of the acoustic wave envelope. From a Fourier transform of the data in the figure, we determined the longitudinal speed of sound in isopropanol to be 1170 m/s at room temperature, in agreement with the literature data. Figure 3(b) shows thermal data using $\lambda_e = 1480$ μm and $\lambda_p = 808$ nm at a grating spacing of $\Lambda = 17.48$ μm. Fitting the data of the figure to a simple exponential, we obtain a measured thermal diffusivity of $D = 7.4$ m^2/s. Literature values of the room temperature density $\rho = 785$ kg/m^3, specific heat at constant pressure $c_p = 2.56$ J/gK, and thermal conductivity $\kappa = 0.14$ W/mK for isopropyl alcohol yield a literature thermal diffusivity $D = 7.0$ m^2/s, which is within 6% of our measured value.

B. Single Crystal Measurements

$CrCl_3$ is a van der Waals solid with in-plane magnetic anisotropy that holds potential for applications in magneto-optical devices. High-quality single crystal samples of $CrCl_3$ were grown by vacuum sublimation [36]. An as-grown flake was immersed in a small amount of MC704 silicone diffusion pump oil and attached to a sapphire substrate by capillary force in order to obtain better index matching and produce less scattered light. The top of the crystal was then covered by a small dab of the oil and subsequently by a circular glass coverslip. The pump laser wavelength was selected to be 800 nm with approximately 7 mW of power (1.4 μJ/pulse), and the probe diode wavelength was selected to be 635 nm (Thorlabs, L635P5). The pump beam was chopped by a mechanical chopper wheel at 2.5 kHz, while the probe operated at 5 kHz and data were recorded using synchronous delay time scanning and the DAC-based method of Ref. [35]. The setup was aligned such that a relatively clear transmitted beam could be focused into both of the detectors; even though we observed scattered light due to inhomogeneity of the sample, a faintly visible beam could be observed for both ±1 orders of the probe. Acoustic waves for $\Lambda = 24.1$ μm are shown in Fig. 4, where oscillations of frequency 213 MHz are observed, providing a longitudinal acoustic velocity of 4920 m/s and a corresponding longitudinal (Young's) modulus of 72.0 GPa at room temperature.

C. Thin-Film Measurements

Cu was vapor deposited onto a silicon substrate to a ∼3 μm thickness. ISTS measurements were performed using $\lambda_e = 495$ nm excitation and probed using the $\lambda_p = 405$ nm fiber-coupled laser diode described above. The pump power was reduced to 25 mW, i.e., 5 μJ per pulse. The pump was amplitude chopped at 2.5 kHz while the probe operated at 5 kHz with data acquisition proceeding by synchronous delay time scanning. Representative data using 4000 averages per data point at $\Lambda = 8.03$ μm wavelength are shown in Fig. 5(a) along with the corresponding Fourier transform in Fig. 5(b). The data and corresponding Fourier transform of Fig. 5 show the presence of three pseudo-Rayleigh modes. The highest frequency acoustic wave we could detect with this method was at 855 MHz for $\Lambda = 3$ μm acoustic waves in the lowest acoustic branch.

Data from the acoustic wavelengths $\Lambda = 17.5$ μm, 12.6 μm, 10.3 μm, 8.03 μm, 6.83 μm, 6.00 μm, 5.40 μm, 4.99 μm, and 4.47 μm were used to build acoustic dispersion curves of the pseudo-Rayleigh modes, plotted as the measured acoustic velocity versus the product of the wave vector and thin-film thickness qh in Fig. 5(c). The thickness h was extracted using an analysis procedure described in the literature [13] with values for the acoustic velocity in amorphous, rolled copper of $v_{t,\mathrm{Cu}} = 2260$ m/s for the transverse speed of sound, and $v_{l,\mathrm{Cu}} = 5010$ m/s for the longitudinal speed of sound, on a silicon substrate with transverse speed of sound $v_{t,\mathrm{Si}} = 5341$ m/s and longitudinal speed of sound $v_{l,\mathrm{Si}} = 8945$ m/s [13]. We used densities of 8.93 g/cm^3 for Cu and 2.32 g/cm^3 for Si. Lines of best fit to the acoustic dispersion curves yielded a thin-film thickness of $h = 3.2 \pm 0.2$ μm, as shown in Fig. 5(c).

D. General Considerations

Although this technique presents several clear advantages, specifically through the use of less probe power, as well as gaining access to a wide array of affordable laser diodes at various wavelengths, we note that there is a compromise in time spent on measuring the individual points of the time-domain traces in series as opposed to in parallel as is done using CW probing and high bandwidth detectors. This was particularly conspicuous for materials with low thermal expansion coefficients that yielded weaker acoustic and thermal signals. Here, the use of lock-in detection did not significantly improve the SNR, and we suggest

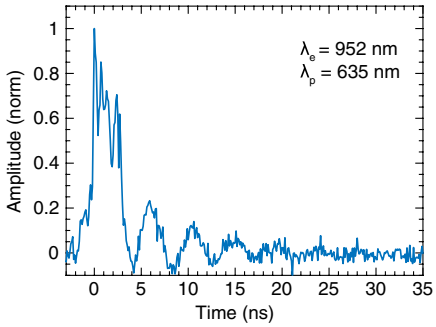

Fig. 6. Response of pulsed laser diode to "excitation" by parasitic backscattered pump light reminiscent of ISTS data. There was no sample in the beam path.

that further development focus on more sensitive detection electronics, such as, e.g., photomultiplier tubes or avalanche photodiodes, in conjunction with attenuated heterodyne detection.

We also note that the coherence lengths of all the diode lasers tested with the pulser were considerably shorter than those derived from their CW operation, necessitating careful selection of optics for the two beams of the probe arm of the experiment. This was discovered by imaging the interference pattern generated by the two probe arms on a bare CCD (Logitech, C170 Webcam with the optics removed) and observing the disappearance of the interference with the addition of a thin (100 μm) piece of glass in one arm relative to the other. Owing to the crudeness of the measurement, we were not able to obtain a reliable estimate of the coherence length. This was especially important for implementation of the attenuated heterodyne, which was not tried here due to lack of ND filters matched in thickness to uncoated substrates. We suggest that custom optics made by coating only one half of a piece of glass by a reflective, attenuating film should allow implementation of this technique.

We also discovered the need to protect the laser diode from scattered stray pump light. For CW output, this was to prevent COD of the laser diode. When the diodes were driven in pulse mode by the T165-2, the effect of the parasitic excitation laser on the diode was to induce a "ringing" feedback in the diode pulser output that was reminiscent of ISTS signals, a representative trace of which is shown in Fig. 6 for $\lambda_e = 952$ nm excitation, $\lambda_p = 635$ nm pulsed laser diode probe, and no sample in the beam path. This occurred for several different combinations of the excitation wavelength and the probe laser diode and only required a small amount of parasitic backscattered light. Although the data in the figure only show an initial sharp response followed by oscillations with no offset, some diodes produced signals that also comprised a decaying background, much like the data of Fig. 4. We addressed this issue by placing filters in front of the laser diode output to permit transmission of the diode wavelength while blocking the pump laser.

4. CONCLUSION

We have demonstrated the use of a laser diode pulser for ultralow-power probing in TG measurements as applied to ISTS. Since the apparatus performs well with very low threshold current laser diodes, the technique may be applied at a variety of probe wavelengths at a fraction of the cost required to perform the same measurements with CW lasers, making it particularly well suited to spectroscopic studies. The acquired data demonstrate that the method can successfully measure the mechanical properties of liquids and single crystals, as well as determine the thickness of a Cu thin film deposited on a silicon substrate. Although not tried here, we suggest that this method could be applied to other experiments where slow dynamics are observed, including, e.g., the propagation of acoustic waves in gas-phase samples, or non-TG measurements of other analogously slow photoinduced dynamics.

Funding. National Science Foundation (DMR-1708929).

Acknowledgment. B.L. and D.H.T. acknowledge Temple University startup funding. M.A. and F.T. were supported by the National Science Foundation through Grant No. NSF/DMR-1708929. We thank Jeff Martoff, Charles Packard, and Jason Tran for assistance with preparation of the copper film.

Disclosures. The authors declare no conflicts of interest.

REFERENCES

1. H. J. Eichler, P. Günter, and D. W. Pohl, *Laser-Induced Dynamic Gratings* (Springer, 2013), Vol. **50**.
2. M. Takezaki, N. Hirota, and M. Terazima, "Nonradiative relaxation processes and electronically excited states of nitrobenzene studied by picosecond time-resolved transient grating method," J. Phys. Chem. A **101**, 3443–3448 (1997).
3. T. Sjodin, H. Petek, and H.-L. Dai, "Ultrafast carrier dynamics in silicon: a two-color transient reflection grating study on a (111) surface," Phys. Rev. Lett. **81**, 5664–5667 (1998).
4. J. Salcedo, A. Siegman, D. D. Dlott, and M. Fayer, "Dynamics of energy transport in molecular crystals: the picosecond transient-grating method," Phys. Rev. Lett. **41**, 131–134 (1978).
5. N. Gedik, J. Orenstein, R. Liang, D. Bonn, and W. Hardy, "Diffusion of nonequilibrium quasi-particles in a cuprate superconductor," Science **300**, 1410–1412 (2003).
6. S. De Silvestri, J. Fujimoto, E. Ippen, E. B. Gamble Jr, L. R. Williams, and K. A. Nelson, "Femtosecond time-resolved measurements of optic phonon dephasing by impulsive stimulated Raman scattering in α-perylene crystal from 20 to 300 K," Chem. Phys. Lett. **116**, 146–152 (1985).
7. T. P. Dougherty, G. P. Wiederrecht, and K. A. Nelson, "Impulsive stimulated Raman scattering experiments in the polariton regime," J. Opt. Soc. Am. B **9**, 2179–2189 (1992).
8. A. Taschin, R. Torre, M. Ricci, M. Sampoli, C. Dreyfus, and R. Pick, "Translation-rotation coupling in transient grating experiments: theoretical and experimental evidences," Europhys. Lett. **56**, 407–413 (2001).
9. R. Torre, A. Taschin, and M. Sampoli, "Acoustic and relaxation processes in supercooled orthoterphenyl by optical-heterodyne transient grating experiment," Phys. Rev. E **64**, 061504 (2001).
10. C. Glorieux, K. Nelson, G. Hinze, and M. Fayer, "Thermal, structural, and orientational relaxation of supercooled salol studied by polarization-dependent impulsive stimulated scattering," J. Chem. Phys. **116**, 3384–3395 (2002).
11. T. Hecksher, D. H. Torchinsky, C. Klieber, J. A. Johnson, J. C. Dyre, and K. A. Nelson, "Toward broadband mechanical spectroscopy," Proc. Natl. Acad. Sci. **114**, 8710–8715 (2017).

12. X. Xu, J. J. A. F. Cuautle, M. Kouyate, N. B. Roozen, J. Goossens, P. Menon, M. K. Malayil, R. Salenbien, R. N. Rajesh, C. Glorieux, P. Griesmar, L. Martinez, and S. Serfaty, "Evolution of elastic and thermal properties during TMOS-gel formation determined by ringing bottle acoustic resonance spectroscopy, impulsive stimulated scattering, photopyroelectric spectroscopy and the hot ball method," J. Phys. D **49**, 085502 (2016).
13. A. R. Duggal, J. A. Rogers, and K. A. Nelson, "Real-time optical characterization of surface acoustic modes of polyimide thin-film coatings," J. Appl. Phys. **72**, 2823–2839 (1992).
14. J. A. Rogers and K. A. Nelson, "Study of Lamb acoustic waveguide modes in unsupported polyimide thin films using real-time impulsive stimulated thermal scattering," J. Appl. Phys. **75**, 1534–1556 (1994).
15. E. Abramson, J. Brown, L. Slutsky, and J. Zaug, "The elastic constants of San Carlos olivine to 17 GPa," J. Geophys. Res. **102**, 12253–12263 (1997).
16. B. Sun, J. Winey, N. Hemmi, Z. Dreger, K. Zimmerman, Y. Gupta, D. H. Torchinsky, and K. A. Nelson, "Second-order elastic constants of pentaerythritol tetranitrate and cyclotrimethylene trinitramine using impulsive stimulated thermal scattering," J. Appl. Phys. **104**, 073517 (2008).
17. A. F. Goncharov, J. Crowhurst, and J. M. Zaug, "Elastic and vibrational properties of cobalt to 120 GPa," Phys. Rev. Lett. **92**, 115502 (2004).
18. J. Janušonis, C.-L. Chang, T. Jansma, A. Gatilova, V. Vlasov, A. Lomonosov, V. Temnov, and R. Tobey, "Ultrafast magnetoelastic probing of surface acoustic transients," Phys. Rev. B **94**, 024415 (2016).
19. C. L. Chang, R. R. Tamming, T. J. Broomhall, J. Janusonis, P. W. Fry, R. I. Tobey, and T. J. Hayward, "Selective excitation of localized spin-wave modes by optically pumped surface acoustic waves," Phys. Rev. Appl. **10**, 034068 (2018).
20. A. J. Schmidt, M. Chiesa, D. H. Torchinsky, J. A. Johnson, A. Boustani, G. H. McKinley, K. A. Nelson, and G. Chen, "Experimental investigation of nanofluid shear and longitudinal viscosities," Appl. Phys. Lett. **92**, 244107 (2008).
21. J. Brown, L. Slutsky, K. Nelson, and L.-T. Cheng, "Velocity of sound and equations of state for methanol and ethanol in a diamond-anvil cell," Science **241**, 65–67 (1988).
22. Z. Dreger, J. Zhou, N. Dang, and Y. Gupta, "Effect of high pressure on acoustic properties of several polymers: use of impulsive stimulated light scattering method," J. Appl. Phys. **109**, 083507 (2011).
23. N. Hemmi, D. Torchinsky, K. Zimmerman, J. Winey, K. Nelson, and Y. Gupta, "Photoacoustic measurements to determine acoustic velocities in shocked condensed materials: application to liquid benzene," Appl. Phys. Lett. **92**, 101926 (2008).
24. J. A. Johnson, A. Maznev, J. Cuffe, J. K. Eliason, A. J. Minnich, T. Kehoe, C. M. S. Torres, G. Chen, and K. A. Nelson, "Direct measurement of room-temperature nondiffusive thermal transport over micron distances in a silicon membrane," Phys. Rev. Lett. **110**, 025901 (2013).
25. C. Hua and A. J. Minnich, "Transport regimes in quasiballistic heat conduction," Phys. Rev. B **89**, 094302 (2014).
26. S. Huberman, R. A. Duncan, K. Chen, B. Song, V. Chiloyan, Z. Ding, A. A. Maznev, G. Chen, and K. A. Nelson, "Observation of second sound in graphite at temperatures above 100 K," Science **364**, 375–379 (2019).
27. O. W. Käding, H. Skurk, A. A. Maznev, and E. Matthias, "Transient thermal gratings at surfaces for thermal characterization of bulk materials and thin films," Appl. Phys. A **61**, 253–261 (1995).
28. J. A. Johnson, A. A. Maznev, M. T. Bulsara, E. A. Fitzgerald, T. Harman, S. Calawa, C. Vineis, G. Turner, and K. A. Nelson, "Phase-controlled, heterodyne laser-induced transient grating measurements of thermal transport properties in opaque material," J. Appl. Phys. **111**, 023503 (2012).
29. M. J. Banet, M. Fuchs, J. A. Rogers, J. H. Reinold Jr, J. M. Knecht, M. Rothschild, R. Logan, A. Maznev, and K. A. Nelson, "High-precision film thickness determination using a laser-based ultrasonic technique," Appl. Phys. Lett. **73**, 169–171 (1998).
30. G. D. Goodno, G. Dadusc, and R. D. Miller, "Ultrafast heterodyne-detected transient-grating spectroscopy using diffractive optics," J. Opt. Soc. Am. B **15**, 1791–1794 (1998).
31. A. Maznev, T. Crimmins, and K. Nelson, "How to make femtosecond pulses overlap," Opt. Lett. **23**, 1378–1380 (1998).
32. P. Epperlein and O. Martin, "Reflectance modulation studies on laser diode mirrors," Inst. Phys. Conf. Ser. **120**, 353–358 (1992).
33. F. Houle, D. Neiman, W. Tang, and H. Rosen, "Chemical changes accompanying facet degradation of AlGaAs quantum well lasers," J. Appl. Phys. **72**, 3884–3896 (1992).
34. M. Hempel, M. Ziegler, J. W. Tomm, T. Elsaesser, N. Michel, and M. Krakowski, "Time-resolved analysis of catastrophic optical damage in 975 nm emitting diode lasers," Appl. Phys. Lett. **96**, 251105 (2010).
35. C. A. Werley, S. M. Teo, and K. A. Nelson, "Pulsed laser noise analysis and pump-probe signal detection with a data acquisition card," Rev. Sci. Instr. **82**, 123108 (2011).
36. M. Abramchuk, S. Jaszewski, K. R. Metz, G. B. Osterhoudt, Y. Wang, K. S. Burch, and F. Tafti, "Controlling magnetic and optical properties of the van der Waals crystal via mixed halide chemistry," Adv. Mater. **30**, 1801325 (2018).

138.167.54.243 (as 2020-01-29 09:17:12)